NEW MEASUREMENT APPROACHES FOR FILM THICKNESS AND WALL TEMPERATURE IN FALLING FILM HEAT EXCHANGERS

A. Åkesjö*, L. Olausson, L. Vamling, M. Gourdon
*Author for correspondence
Division of Industrial Energy Systems and Technologies, Department of Energy and Environment
Chalmers University of Technology,
Göteborg, 412 96,
Sweden,
E-mail: anders.akesjo@chalmers.se

ABSTRACT

Falling film evaporation is used in various fields, e.g. food and pulp & paper industry. Evaporation is very energy intense and relatively small efficiency improvements to the techniques can lead to large savings in absolute numbers. Falling film evaporation is affected by the wave dynamics; hence further knowledge of the behaviour of the liquid film flow can promote efficiency improvements.

In this work, two new measurement approaches have been investigated. The first approach is to use a laser triangulation scanner combined with a high-speed camera where the laser scanner continuously measures the film thickness along a vertical line, resolving the flow pattern in high detail. The second approach is to measure local wall temperatures, enabling calculation of local heat transfer coefficients at any desired location.

These methods has been tested and evaluated in a falling film test facility. Both approaches have proven to give valuable insights into the process and the results are in good agreement with literature data.

INTRODUCTION

Falling film evaporation is a proven and reliable thermal separation technique. In falling film heat exchangers, the liquid flows in a thin falling film along a solid surface. Falling film evaporation, as all thermal separation techniques, is inherently energy intensive. Thus, improving the energy efficiency of the technique can substantially improve the overall energy economy. Falling film evaporators are characterized by high heat transfer at relatively low mass flow rates and small temperature differences. Together with the short product residence time, it gives falling film evaporators unique advantages. The technique is used for heat-sensitive fluids such as fruit juice, sugar and dairy products, where short residence time and close temperature controls during the heat transfer process are essential. Falling film evaporation is also widely used in the pulping industry. Typically, the viscosities of the final products are considerably higher than the viscosity of water.

NOMENCLATURE

A	[m^2]	Area
c_p	[J/kgK]	Specific heat capacity
d	[m]	Diameter
g	[m/s^2]	Gravitational acceleration
h	[W/m^2K]	Heat transfer coefficient
k	[W/mK]	Thermal conductivity
Ka	[-]	Kapitza number
L	[m]	Length
Nu	[-]	Nusselt number
Pr	[-]	Prandtl number
Q	[W]	Power supplied
Re	[-]	Reynolds number
T	[K]	Temperature
x	[m]	Cartesian axis direction
z	[m]	Cartesian axis direction

Special characters

Γ	[$kgm^{-1}s^{-1}$]	Mass flow rate per unit width
δ	[m]	Film Thickness
μ	[kg/(s·m)]	Dynamic viscosity
ν	[m^2/s]	Kinematic viscosity
ρ	[kg/m^3]	Density
σ	[N/m]	Surface tension

Subscripts

b	Bulk
l	Local
i	Interface
o	Outside
r	Reference
w	Wall

Characterization of the flow in falling films is often described using dimensionless numbers. The most important ones are the Reynolds number (Re), the Kapitza number (Ka), the Nusselt number (Nu), and the Prandtl number (Pr), defined as follows:

$$\mathrm{Re} = \frac{4\Gamma}{\mu} \tag{1}$$

$$\mathrm{Ka} = \frac{\mu^4 g}{\rho\sigma^3} \tag{2}$$

$$\mathrm{Nu} \equiv \frac{h}{k}\left(\frac{\nu^2}{g}\right)^{1/3} \tag{3}$$

$$\mathrm{Pr} \equiv \frac{c_p \mu}{k} \tag{4}$$

where Γ is the specific mass flow rate per unit circumference, μ is the dynamic viscosity, g is the gravitational acceleration, ρ is the density, σ is the surface tension, h is the heat transfer coefficient, k is the thermal conductivity, v is the kinematic viscosity and c_p is the specific heat capacity.

The hydrodynamics of falling films has been a research topic of several researchers, e.g. [1], [2] and [3]. The flow patterns are usually characterized by the degree of turbulence in the liquid phase [4]. The transitions between the different flow regimes are often described as a function of the Reynolds and Kapitza number. Al-Sibai [5] developed models for the transitions under non-evaporative conditions. The flow was mapped into five different zones, Laminar (L), Sinus-shaped waves (S), Wavy-laminar (WL), Transition region (TR) and Turbulent (T). These regimes describe how the flow transitions from being a smooth film to develop sinusoidal waves that transitions into 2D and later 3D waves, lastly having a fully turbulent, chaotic behaviour. Each zone obviously impacts the hydrodynamics in different ways.

Numerous studies have also been dedicated to determine the local film thickness of the liquid film in different flow regimes and a large variety of techniques exits. Simple methods such as drainage or hold-up [6] where the flow is cut-off and the liquid on the surface is collected and measured yielding an average film thickness. Shadow photographs are also used, where the film thickness is estimated from images. Micrometre screw or needle-contact-probe [7] has also been used to measure the thickness in a single point. There are also more advanced methods e.g. High Frequency Needle Probes [8], measuring the changes of impedance in the liquid film due to different thicknesses.

All techniques have their pros and cons; however, generally they yield low accuracy or disturb the flow directly or indirectly due to the need of adding additives to the liquid for the method to work. In addition, most of the techniques are only capable of determining an average film thickness or a thickness in a single point yielding no information about how the flow changes over a distance.

The film thickness for flat laminar falling films without surface evaporation can be obtained from the Nusselt's film theory as [9]:

$$\delta_{Nusselt} = \left(\frac{3\nu^2 \,\mathrm{Re}}{4g} \right)^{1/3} \tag{5}$$

Lukach et al. proposed the following correlation for the mean film thickness under wavy-laminar conditions [10]

$$\delta_{Lukach} = 0.805 \left(\frac{\nu^2}{g} \right)^{1/3} \cdot \mathrm{Re}^{0.368} \tag{6}$$

and Brötz [11] proposed the following correlation for turbulent conditions:

$$\delta_{Brötz} = 0.068 \left(\frac{\nu^2}{g} \right)^{1/3} \cdot \mathrm{Re}^{2/3} \tag{7}$$

The heat transfer in falling film is usually described as a function of the Reynolds and Prandtl number. The heat transfer is usually described by two separate correlations; a laminar and a turbulent. The influence of each dimensionless number depends on the flow regimes. For truly laminar flow the heat transfer occurs by pure conduction and is rate-determined by the film thickness and thus decreases with the Reynolds number. In the turbulent region, however, the Nusselt number increases with the Reynolds number [12]. For the intersection (transitional region) between the two a superposition is often used. Schnabel and Schlünder [13] developed correlations for both evaporative and non-evaporative conditions under constant heat flux.

$$Nu_{Evaporation} = \sqrt{Nu_{lam}^2 + Nu_{turb}^2} \tag{8}$$

$$Nu_{lam} = 1.43 \cdot \mathrm{Re}^{-1/3} \tag{9}$$

$$Nu_{turb} = 0.0036 \cdot \mathrm{Re}^{0.4} \cdot \mathrm{Pr}^{0.65} \tag{10}$$

$$Nu_{Heating} = \max \begin{cases} 2.27 \cdot \mathrm{Re}^{-1/3} \\ 0.94 \cdot \sqrt[3]{\mathrm{Re}^{1/3} \cdot \mathrm{Pr} \cdot \left(\frac{\nu^2}{g} \right)^{1/3} \Big/ L_H} \\ 0.032 \cdot \mathrm{Re}^{0.2} \cdot \mathrm{Pr}^{0.344} \\ 0.0078 \cdot \mathrm{Re}^{0.4} \cdot \mathrm{Pr}^{0.344} \end{cases} \tag{11}$$

Based on these studies it can be concluded, for moderate Reynolds number, that the heat transfer coefficients have similar trends for evaporating and non-evaporating conditions. This enables the results based on subcooled liquid conditions to analogously be interpreted for evaporative conditions.

Local heat transfer measurements are typically performed by measuring the temperature difference between the wall and the bulk. Usually the most difficult is to obtain the surface temperature which for example can be measured by installing a thermocouple (e.g. by soldering) inside the tube wall. However, this approach requires much work, the number of measurement points is limited, and the position of the thermocouples has to be predetermined.

The objective of this work was to investigate two new experimental approaches for characterizing falling films which would help to gain understanding of the hydrodynamics and heat transfer of falling films and the interaction thereof. This was done in an available experimental setup. A quantitative method for obtaining wave characteristics and film thicknesses over a section of the surface is assessed. Secondly, and in parallel, a method to obtain local wall surface temperatures in order to obtain local heat transfer coefficients is evaluated.

EXPERIMENTAL

Experimental Setup

The experimental setup consist of a copper tube, open to the atmosphere, of length L = 0.8 m, outer diameter d_o= 60 mm and 5 mm thickness. In Figure 1, a schematic overview of the experimental setup and the equipment used for the film visualization is presented. To be able to visually examine the flow, the product flows on the outside of the tube and is heated from the inside by an electrical heater. The heat transfer surface is $A_o = 0.15$ m^2. The flow is distributed using a specially designed overflow distributer to achieve an even liquid film on the tube. Temperature, flow rate, density, viscosity and supplied power to the heater are measured online, see Table 1.

Table 1: Measurement equipment.

Quantity	Instrument	Accuracy
Temperature	PT-100, ABB H210, H600	± 0.2 K
Mass flow rate and density	Endress + Hauser PROline promass 80 H	± 0.20 % of range
Viscosity	Marimex, Viscoscope – Sensor VA-300L	± 1.0 % of value
Power	Carlo Gavazzi, Energy Analyser WM22-DIN	± 50 W

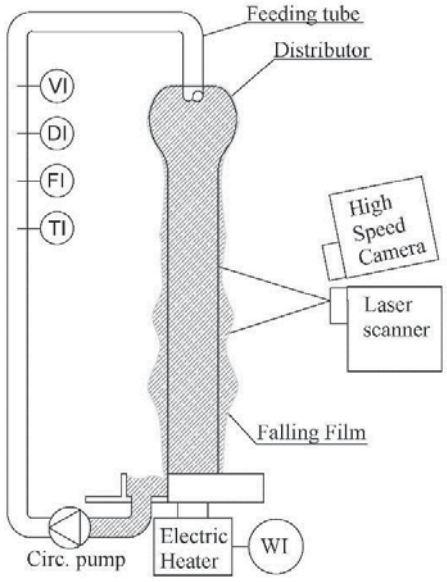

Figure 1 Schematic diagram of the evaporator setup: DI= Density meter, FI=Flow meter, TI=Temperature meter, VI=viscometer, WI=Power supplied.

Film Visualization

The new film visualization approach is using an optical triangulation scanner (light intersection method) of the model scanCONTROL 2950-100 from Micro-Epsilon [14]. The scanner uses a 20 mW power source to project a laser beam of wave length 658 nm onto the target surface. A sensor matrix detects the diffused light and measures the reflected angle in 1280 points along the projected line. The angle is used to calculate the distance z to the surface and with an inbuilt camera the scanner also determine the length x of the laser beam which is dependent on the distance z, see Figure 2. The scanner samples at a frequency of 500 Hz with a resolution of ± 1.2·10^{-5} m and a nonlinearity, i.e. deviation from true value, of ± 0.16 % based on the full scale output [14].

The scanner is used to continuously measure the distance $z_i(x)$ to the liquid-gas interface along a vertical path. By also measuring a reference distance $z_r(x)$ between the scanner and a clean surface without any flow, the thickness of the liquid film in each point can be calculated as $\delta(x) = z_r(x) - z_i(x)$. By doing this, and also since the film thickness is small, the influence of the scanners nonlinearity is reduced, resulting in higher measurement accuracy.

Simultaneous with the film thickness measurements, high-speed images were also taken with the same sampling frequency for comparison.

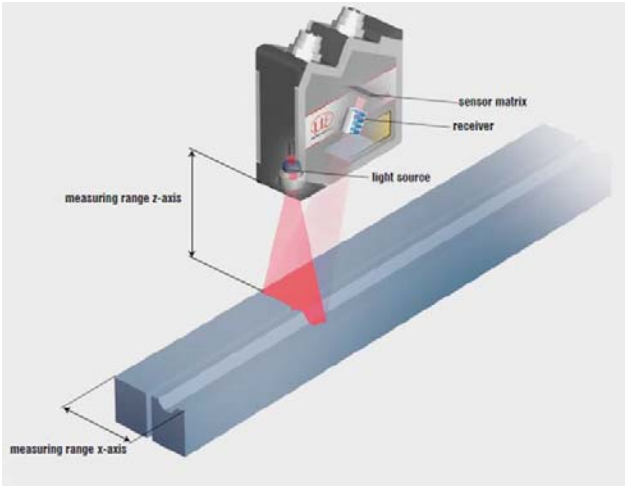

Figure 2 Image from the manufacturer demonstrating the working principle of the laser-scanner.

The measured distances are collected and stored into text files with all 1280 *z(x)* points as columns and the number of rows being dependent on the sampling time. The measurements were imported to MATLAB and there the data was filtered with a standard local regression technique using weighted linear least squares. The reason for this was to get rid of unwanted noise cause by the strong light [15] used for the high-speed camera and occasional misreading such as droplets that could have been picked up by the scanner instead of the film thickness.

The treated data from the scanner was then compiled with the high-speed images into parallel, synchronized movies. These movies yield a detailed and comprehensive view of the liquid film and both the movement and wave structures can be followed in time over the measurement distance. The film thickness measurement also enables the quantitative determination of important film characteristics such as wave amplitude, average film thickness etc.

Local Temperature Measurements

The new approach to measure local wall temperatures utilizes the principle of a copper-constantan thermocouple. In this case, however, the copper tube act as one of the conductors and the junction is created by pointing a constantan needle at any desired location and thus the local temperature is obtained. See Figure 3 for a picture of the needle and the copper tube.

The system has been calibrated by using an accurate quartz thermometer to acquire the real temperature yielding a correction function for the constantan needle temperature measurement.

Figure 3 Image showing the constantan needle measuring the tube wall temperature.

To further assure correct measurement of the wall temperature, thermocouples has been inserted in three chordally drilled holes at different positions. These thermocouples have also been calibrated according to the same procedure described above and they have been used to compare the results with the constantan needle measurements. These thermocouples were not used during the experiments since the outgoing cable would disturb the flow profile on the tube. However, a comparative experiment revealed that the maximum deviation between the different approaches was smaller than 0.05 K, indicating a reliable measurement of the tube wall temperature. The total inaccuracy of the temperature measurements with the constantan needle has therefore been estimated to ± 0.13 K.

Once the wall temperature is obtained, a small amount of the liquid film can be collected at the same location and the temperature of the bulk can be measured. With the power supplied by the electrical heater, local heat transfer coefficients are obtained as follows:

$$h_l = \frac{Q}{A\left(T_w - T_b\right)} \tag{12}$$

where Q is the supplied power, A is the surface area and T_w and T_b are wall respectively bulk temperature.

METHODS AND MATERIALS

The performance of the two new approaches was investigated on a wide range of flow regimes. This was achieved by mixing water with different fractions of dairy powder. Adding dairy powder increases the density and viscosity, hence reducing the Reynolds and increasing Kapitza number making it possible to investigate flow regimes from wavy-laminar up to fully turbulent. In Figure 4 the experimentally investigated points are presented in the flow map proposed by Al-sibai [5].

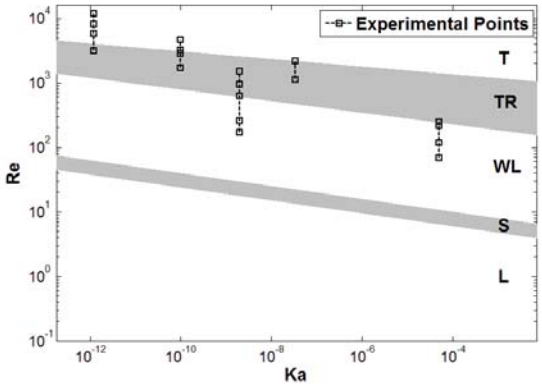

Figure 4 Distribution of measurements points in flow regimes. The regimes in the figure are according to Al-Sibai [5], Laminar (L), Sinus-shaped waves (S), Wavy-laminar (WL), Transition region (TR) and Turbulent (T).

The fluid was recirculated over the tube and heated by the electrical heater, supplying a constant power of 1.5 kW. The inlet temperature was maintained at 50 °C. Several flow rates were investigated and surface and bulk temperatures were measured at three different locations spread along the whole tube. The film visualization method was applied in an area approximately 60-160 mm from the inlet.

RESULTS AND DISCUSSION

Laser scanner

Visualization movies have been compiled for all experimental points and two snapshots from one of them at Ka=$5\cdot10^{-5}$ and Re=70 can be seen in Figure 5. In the figure, it can be seen that the laser scanner is able to detect the liquid film flow and capture the wave dynamics in the same way as the high speed images does. The laser is capable of detecting the wave amplitude and it is possible to observe the movement and changes to the waves. It is also possible to see the hint of the backflow phenomena occurring before the wave often described in the literature (e.g. [16]), even though the applied filter has made them less clear. Besides this, the filtering technique works as anticipated. Occasional falling droplets did never appear to be a problem. Shadow effects, a phenomenon were the measuring target is shadowing some parts of itself from the measurement [14], were not a problem during the measurements but could potentially become a problem in other setups and therefore one should be aware of this.

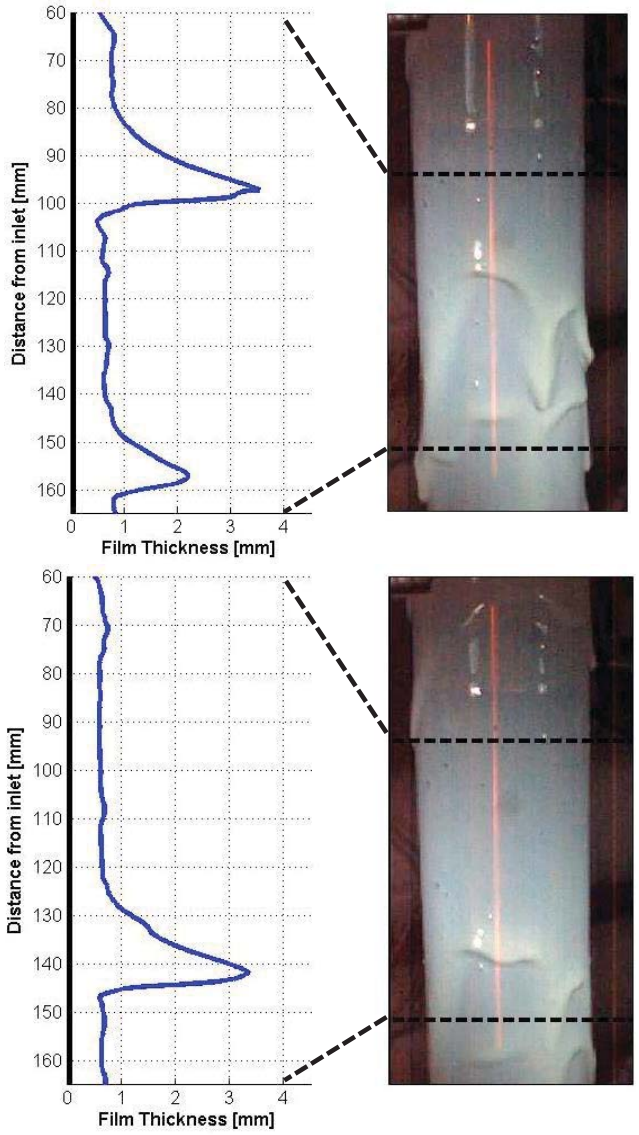

Figure 5 Two snapshots from the compiled movie at Ka=$5\cdot10^{-5}$ and Re=70. Left figures are from the laser scanner, right figures from the high-speed imaging system. The time difference between the snapshots is 0.084 s.

The average film thickness value has been calculated from the movies and a comparison between these values and the correlations presented in eqs. 5-7 can be seen in Table 2 and 3.

From Table 2 it is clear that the laser scanner has problems with detecting pure water as the film thickness is significantly underestimated in the measurements compared to the correlations. This was an expected result, occurring as a consequence of the transparency of the water film. The results in Table 3, however, show that the laser measurement performs better when dairy powder is added, increasing the opacity of the fluid. The Kapitza number is increasing with increasing concentration of the dairy product, and thus so should the opacity. For the lowest concentration at Ka=$1\cdot10^{-10}$, the measurements are seen to somewhat underestimate the film thickness, which could imply that the laser measures at a certain depth into the film. For all the higher concentrations (higher Ka-numbers), the measurement are in better agreement with the correlations. For points in the wavy-laminar region (WL), the correlation by Lukach is the most applicable, whereas points in the transitions region (TR) could be compared with both the correlation by Brötz and Lukach. This indicates that the principle of measuring the film thickness can be trusted. However, since the actual film thickness is done in two steps, subtracting $z_i(x)$ from $z_r(x)$, it is of highest importance that the scanner and the tube are properly fixed and do not move in between the measurements to yield high accuracy.

Table 2: Measured and correlated film thickness in mm (according to eq.5-7) for water at different Reynolds numbers.

Ka	Re	Regime	Meas.	Nusselt	Lukach	Brötz
$1\cdot10^{-11}$	3200	TR	0.21	0.42	0.50	0.46
$1\cdot10^{-11}$	5800	T	0.25	0.50	0.60	0.65
$1\cdot10^{-11}$	8100	T	0.34	0.56	0.68	0.82
$1\cdot10^{-11}$	11600	T	0.41	0.63	0.77	1.04

Table 3: Measured and correlated film thickness in mm (according to eq.5-7) for water-dairy powder mixtures at different Kapitza and Reynolds numbers.

Ka	Re	Regime	Meas.	Nusselt	Lukach	Brötz
$1\cdot10^{-10}$	1700	TR	0.34	0.52	0.60	0.46
$1\cdot10^{-10}$	2800	TR	0.46	0.62	0.72	0.65
$1\cdot10^{-10}$	3300	T	0.50	0.74	0.86	0.82
$1\cdot10^{-10}$	4600	T	0.70	0.83	0.99	1.04
$2\cdot10^{-9}$	170	WL	0.21	0.38	0.24	0.16
$2\cdot10^{-9}$	260	WL	0.34	0.44	0.28	0.21
$2\cdot10^{-9}$	630	TR	0.48	0.55	0.37	0.35
$2\cdot10^{-9}$	900	TR	0.56	0.63	0.43	0.46
$2\cdot10^{-9}$	1500	TR	0.66	0.76	0.52	0.65
$3\cdot10^{-8}$	1100	TR	1.18	1.82	1.30	2.25
$3\cdot10^{-8}$	1400	TR	1.22	1.95	1.40	2.61
$5\cdot10^{-5}$	70	WL	0.93	1.85	1.19	0.89
$5\cdot10^{-5}$	120	WL	1.29	2.44	1.60	1.42
$5\cdot10^{-5}$	220	WL	1.83	3.15	2.12	2.25
$5\cdot10^{-5}$	250	TR	2.08	3.52	2.38	2.61

Temperature measurements

The Nusselt number has been calculated for the three different points along the heat transfer surface where the temperature was measured. The result for the water experiments are shown in Figure 6 together with the heat transfer correlations for evaporating and heating conditions presented in eqs. 8-11. The measurements were performed at a distance of 0.1 (Nu1), 0.3 (Nu2) and 0.6 (Nu3) m from the inlet.

The measured points fit well with $Nu_{Heating}$-correlation for the entire range of Reynolds numbers. For higher values, however, the spread of the points is larger. This is a result of

higher heat transfer coefficients implying the measurement of smaller temperature difference which inherently yields higher measurement uncertainty. The error bars included in Figure 6 display the aggregated uncertainties in the determination of the heat transfer coefficient, including the heat flux and temperature measurements. Even if the trend is the same for all different measurement positions the behaviour is somewhat different, indication that the local heat transfer coefficient varies along the tube. The level for the $Nu_{Evaporation}$-correlation is lower, however following the same trend with the Reynolds number.

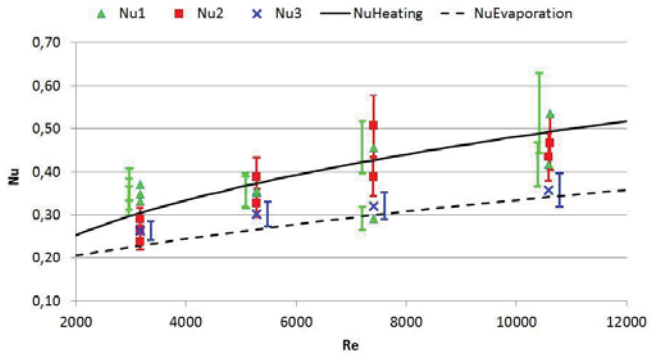

Figure 6 Nusselt number as a function of Reynolds number for three different points along the heat transfer surface for water with error bars. To increase readability, Nu1's error bars are shifted to the left of each point, and correspondingly, Nu3's error bars are shifted to the right. The solid and dashed lines represent the correlated heat transfer for heating and evaporation using eqs. 8-10 and 11.

In Figure 7, similarly, the Nusselt-number is displayed as a function of the Reynolds number for the water-dairy powder mixture having $Ka=1\cdot10^{-10}$.

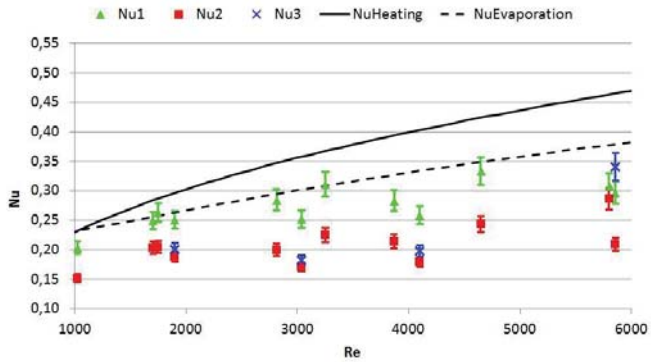

Figure 7 Nusselt number as a function of Reynolds number for three different points along the heat transfer surface for a water-dairy powder mixture ($Ka=1\cdot10^{-10}$) with error bars. The solid and dashed lines represent the correlated heat transfer for heating and evaporation using eqs. 8-10 and 11.

These measurements do not agree to the same extent as with water. The trend is the same but the correlations generally over-predict the measured heat transfer values. According to the flow map in figure 4, all these points should be in the transition region or turbulent region. However, when examining the movies generated from the film visualization method, the flow does not appear to have a large turbulent component; rather it is closer to laminar conditions. This could be an explanation for why the heat transfer values do not agree as well with the correlation as water. For measurements done at higher Kapitza numbers, the calculated Nusselt numbers are again closer to the value given by the heating correlation. There, the observed regime is also closer to what is predicted by Figure 4. This emphasizes the benefits of using both the new measurement approaches together.

CONCLUSION

The presented new measurement approaches have shown to work as intended, yielding results with reasonable accuracy for this type of application. The film thickness measurement can be used to study the flow in detail. Based on the laser measurement approach, it is possible to further interpret the data using statistical analysis, obtaining properties such as: base film thickness, wave occurrences, wave velocity. The heat transfer measurement can be used to study the local heat transfer in more detail.

REFERENCES

1. Kapitza, P.L. and S.P. Kapitza, Collected papers of P. L. Kapitza (Edited by D. T. Haar). Pergamon Press Oxford, 1964.
2. Patnaik, V. and H. Perez-Blanco, Roll waves in falling films: an approximate treatment of the velocity field. International Journal of Heat and Fluid Flow, 1996. 17(1): p. 63-70.
3. Kunugi, T. and C. Kino, DNS of falling film structure and heat transfer via MARS method. Computers & Structures, 2005. 83(6–7): p. 455-462.
4. Grossman, G. and M.T. Heath, Simultaneous heat and mass transfer in absorption of gases in turbulent liquid films. International Journal of Heat and Mass Transfer, 1984. 27(12): p. 2365-2376.
5. Al-Sibai, F., Experimentelle Untersuchung der Strömungscharakteristik und des Wärmeübergangs bei welligen Rieselfilmen, in Fakultät für Maschinenwesen. 2005, RWTH Aachen: Aachen.
6. Portalski, S., Studies of falling liquid film flow: Film thickness on a smooth vertical plate. Chemical Engineering Science, 1963. 18(12): p. 787 -804.
7. Takahama, H. and S. Kato, Longitudinal flow characteristics of vertically falling liquid films without concurrent gas flow. International Journal of Multiphase Flow, 1980. 6(3): p. 203-215.
8. Aviles, M.L., Experiments on falling film evaporation of a water-ethylene glycol mixture on a surface with longitudinal grooves, in Institut für Energietechnik. 2007, Technischen Universität Berlin.
9. Schnabel, G. and J.W. Palen, Wärmeubergang an senkrechten berieselten Flächen. VDI Wärmeatlas, 8th Edition, Springer-Verlag Berlin, Sect. Md, 1998.

10. Lukach, Y.Y., L.B. Radchenko, and Y.M. Tananayiko, Determination of the average thickness of a film of water during gravitation of flow along the exterior surface of vertical polymeric pipes. International Chemical Engineering, 1972. 12: p. 517-519.
11. Brötz, W., Predetermination of absorption rate of gases in flowing liquid layers (Über die Vorausberechnung der Absorptionsgeschwindigkeit von Gasen in strömenden Flüssigkeitsschichten). Chemie-Ingenieur-Technik, 1954. 26: p. 470-478.
12. Numrich, R., Heat transfer for falling film evaporation. Wärmeübergang bei der Fallfilmverdampfung, 1992. 27(5): p. 331-335.
13. Schnabel, G. and E.U. Schlünder, Wärmeübergang von senkrechten Wänden an nichtsiedende und siedende Rieselfilme. "Heat Transfer from Vertical Walls to Falling Liquid Films with or Without Evaporation." Verfahrenstechnik, 1980. 14(2): p. 79-83.
14. Micro-Epsilon. Laser-Scanner Manual. [cited 2015 25 February]; Available from: http://www.micro-epsilon.com/download/manuals/man--scanCONTROL-29xx--en.pdf.
15. Blanco, D., et al., Influence of Ambient Light on the Quality of Laser Digitized Surfaces, in Advances in Electrical Engineering and Computational Science, S.-I. Ao and L. Gelman, Editors. 2009, Springer Netherlands. p. 447-457.
16. Dietze, G.F., A. Leefken, and R. Kneer, Investigation of the backflow phenomenon in falling liquid films. Journal of Fluid Mechanics, 2008. 595: p. 435–459.